Pseudorotor-Flux-Oriented Control of an Induction Machine for Deep-Bar-Effect Compensation

Jul-Ki Seok, *Student Member, IEEE*, and Seung-Ki Sul, *Senior Member, IEEE*

***Abstract*— In an induction machine with deep rotor bars, the rotor parameters change due to skin effect and saturation, and the skin effect is often modeled as a ladder network. For the high-performance drive of an induction machine with deep bars, many sophisticated control strategies and machine models have been discussed. As a control strategy, a complicated airgap flux-oriented control scheme is mostly adopted, because it is not possible to define a unique rotor flux in deep bar model. However, a unique pseudorotor flux can be defined, and it is straightforward to achieve independent control of pseudorotor flux and torque. This control scheme can be applied to any nth multiple ladder network. In this paper, it is described how a deep-bar effect of an induction machine can be negligible by performing the proper field-oriented control. By using the concept of pseudorotor flux, the conventional rotor-flux-oriented control using equivalent rotor parameters is effective for deep-bar and/or double-cage machines. The actual insulated gate bipolar transistor (IGBT) inverter systems with a high-precision torque transducer are implemented and thoroughly tested on a 250-hp induction machine and a 5.5-kW double-cage induction machine to confirm their validity.**

***Index Terms*—Deep rotor bars, pseudorotor flux, skin effect.**

I. Introduction

FOR many mechanical systems, it has been well known that a variable-speed drive will provide improved performance, productivity, and energy efficiency. Therefore, variable-speed drives are being increasingly designed into new systems and are also being fitted to existing systems. In general, the induction machines for variable-speed drives should be designed to have a rotor resistance as low as possible to minimize losses [1]. In contrast with a general purpose induction machine, there is no need to compromise the design of the rotor bar shape in order to achieve adequate starting torque. However, in large machines, such as mill drive systems, the rotor bar is also large to incorporate high rotor current.

Until now, it has been known that the rotor deep-bar effect can have a significant influence on the effective rotor time constant of the induction machine. In order to compensate for the deep-bar effect, sophisticated control algorithms and advanced rotor models have been discussed [2]–[6]. De Doncker [4] proposed a double-cage model considering the nonuniform distribution of rotor currents and an airgap flux-oriented control scheme. In that paper, the experimental validation is not given, and the rotor parameters are obtained from traditional locked rotor tests, rated load data, and no-load tests. In the simulation results of that paper, large torque error occurred when a 5-Hz torque command with rectangular shape was applied. However, using equivalent rotor parameters obtained from the pseudorotor-flux-oriented control scheme in our study, the machine torque can respond perfectly to step torque command. Healey *et al.* [5], [6] presented the advanced rotor models, and the rotor parameters are obtained by finite-element method analysis. In that study, the machine torque of the simple model was oscillatory and it took a long time to settle down. This is because the rotor circuit parameters are much detuned and, therefore, the flux is oscillatory. Consequently, in previous studies, the significant rotor deep-bar effect resulted from the rotor parameter detuning effect. In a field-oriented control of an induction machine, the rotor current frequency of the machine is maintained within the rated slip frequency by controlling the stator currents, except for a very short transient state.

In this paper, it is presented that a deep-bar effect is practically negligible when performing the proper field-oriented control of an induction machine. Introducing an indirect pseudorotor-flux-oriented control scheme, the conventional rotor-flux-oriented control using equivalent rotor parameters is effective for deep-bar and/or double-cage machines. The validity of the study is verified for insulated gate bipolar transistor (IGBT) inverter-fed induction machine drive systems with a high-precision torque transducer, and they are thoroughly tested on a 250-hp induction machine for field-oriented control operation. In order to show clearly the effectiveness of the proposed approach, some tests are performed on a 5.5-kW double-cage induction machine, the impedance locus of which fits closely to that of the deep-bar machine.

II. Deep-Bar Model

For easy understanding of the deep-bar effect, the rotor deep bar may be modeled using a double-cage model; the steady state equivalent circuit is shown in Fig. 1.

The rotor voltage equations of the double-cage model and the torque quantity are given as follows [4]:

$$0 = r_1 i_{d1}^e + p\lambda_{d1}^e - \omega_{sl}\lambda_{q1}^e \tag{1}$$

$$0 = r_1 i_{q1}^e + p\lambda_{q1}^e + \omega_{sl}\lambda_{d1}^e \tag{2}$$

Paper IPCSD 97–74, presented at the 1996 Industry Applications Society Annual Meeting, San Diego, CA, October 6–10, and approved for publication in the IEEE TRANSACTIONS ON INDUSTRY APPLICATIONS by the Industrial Drives Committee of the IEEE Industry Applications Society. Manuscript released for publication December 8, 1997.

J.-K. Seok is with the Production Engineering Center, Samsung Electronics Company, Ltd., Suwon City, Kyungki-Do, 442-742 Korea.

S.-K. Sul is with the Department of Electrical Engineering, Seoul National University, Seoul, 151-742 Korea.

Publisher Item Identifier S 0093-9994(98)03620-2.

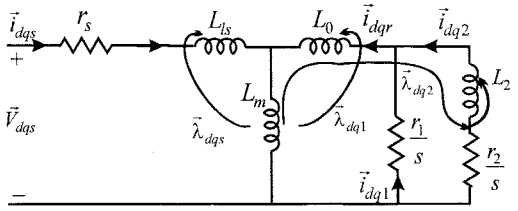

Fig. 1. Equivalent circuit of steady-state double-cage induction machine.

$$0 = r_2 i^e_{d2} + p\lambda^e_{d2} - \omega_{sl}\lambda^e_{q2} \tag{3}$$

$$0 = r_2 i^e_{q2} + p\lambda^e_{q2} + \omega_{sl}\lambda^e_{d2} \tag{4}$$

$$T_e = \frac{3P}{4}|\overline{\lambda}_{dqs} \times \bar{i}_{dqs}|. \tag{5}$$

In the above equations, $i^e_{d1}, i^e_{q1}, i^e_{d2}$, and i^e_{q2} indicate the d- and q-axes upper cage and lower cage rotor currents, respectively. $\lambda^e_{d1}, \lambda^e_{q1}, \lambda^e_{d2}$, and λ^e_{q2} represent the d- and q-axes pseudo and lower cage total rotor flux, respectively. $\overline{\lambda}_{dqs}$ and $\bar{i}_{dqs}$ are the stator flux linkage and the stator current space vector, respectively. ω_{sl} is the rotor electrical slip angular velocity, and p indicates the differential operator. r_1 is the upper cage rotor resistance, r_2 is the lower cage rotor resistance, and P represents the number of poles. $\overline{V}_{dqs}$ denotes the stator voltage space vector, r_s is the stator resistance, and L_{ls} is the stator leakage inductance, respectively.

The flux linkages are expressed as the functions of the rotor and stator currents:

$$\overline{\lambda}_{dqs} = (L_m + L_{ls})\bar{i}_{dqs} + L_m\bar{i}_{dqr} = L_s\bar{i}_{dqs} + L_m\bar{i}_{dqr} \tag{6}$$

$$\overline{\lambda}_{dq1} = L_m\bar{i}_{dqs} + (L_m + L_0)\bar{i}_{dqr} \tag{7}$$

$$\overline{\lambda}_{dq2} = L_m\bar{i}_{dqs} + (L_m + L_0)\bar{i}_{dqr} + L_2\bar{i}_{dq2}. \tag{8}$$

In the above equations, L_m is the mutual inductance, and L_0, L_2 represent the leakage inductance of each cage, respectively.

III. Pseudorotor Flux-Oriented Control of Deep-Bar Model

In previous studies [4]–[6], the airgap flux-oriented control scheme is adopted because it is not possible to define a unique rotor flux linkage space vector in deep-bar and/or double-cage model. However, it is already known that rotor-flux-oriented control has a simpler structure and a more effective decoupling characteristic than airgap flux-oriented control [7]. In the deep-bar and/or double-cage model, a unique pseudorotor flux linkage vector $\overline{\lambda}_{dq1}$ can be defined, and it is straightforward to achieve independent control of pseudorotor flux and torque. This control scheme can be applied to any nth multiple ladder network.

From (7), the total rotor current space vector is as follows:

$$\bar{i}_{dqr} = \frac{\overline{\lambda}_{dq1} - L_m\bar{i}_{dqs}}{(L_m + L_0)}. \tag{9}$$

Substituting (9) for (6), the stator flux linkage vector is alternatively expressed as

$$\overline{\lambda}_{dqs} = \left(L_s - \frac{L_m^2}{L_m + L_0}\right)\bar{i}_{dqs} + \frac{L_m}{L_m + L_0}\overline{\lambda}_{dq1}. \tag{10}$$

By applying (10) into (5), the electromagnetic torque equation (11) is represented by pseudorotor flux linkage vector $\overline{\lambda}_{dq1}$ and stator current vector $\bar{i}_{dqs}$ in an arbitrary reference frame. This expression is valid for an induction machine having sinusoidal distributions of flux and current density, regardless of the number of rotor branches:

$$\begin{aligned} T_e &= \frac{3P}{4}|\overline{\lambda}_{dqs} \times \bar{i}_{dqs}| \\ &= \frac{3P}{4}\left|\left\{\left(L_s - \frac{L_m^2}{L_m + L_0}\right)\bar{i}_{dqs} + \frac{L_m}{L_m + L_0}\overline{\lambda}_{dq1}\right\} \times \bar{i}_{dqs}\right| \\ &= \frac{3P}{4}\,\frac{L_m}{L_m + L_0}|\overline{\lambda}_{dq1} \times \bar{i}_{dqs}|. \end{aligned} \tag{11}$$

The independent control of torque and flux is accomplished by choosing the synchronous angular velocity to be the instantaneous speed of $\overline{\lambda}_{dq1}$ and locking the phase of the flux to be entirely in the d axis, resulting in

$$\lambda^e_{q1} = 0. \tag{12}$$

In the steady state, the slip relation follows from (2) and (4):

$$\omega_{sl} = \frac{r_1 i^e_{q1}}{\lambda^e_{d1}} = -\frac{r_2 i^e_{q2}}{\lambda^e_{d2}} \tag{13}$$

$$\lambda^e_{d1} = \lambda^e_{d2} = L_m i^e_{ds}. \tag{14}$$

From (13) and (14),

$$i^e_{q2} = \frac{r_1}{r_2} i^e_{q1}. \tag{15}$$

Applying (15) and (12) into (13), the slip angular velocity is expressed as

$$\omega_{sl} = \frac{r_1 r_2}{(L_m + L_0)(r_1 + r_2)}\,\frac{i^e_{qs}}{i^e_{ds}}. \tag{16}$$

Equation (16) indicates that the rotor currents are uniformly distributed by the ratio of each branch impedance in steady state, and it is equivalent to the slip equation of the simple model. In other words, the conventional rotor-flux-oriented control can be adopted.

IV. Simulation Results

In a rotor with deep bars, to obtain accurate values of the electromagnetic torque, rotor current, and so on, it is necessary to take into account the skin effect in the machine model. Simulation is performed for the rotor parameters, as shown in Table I, that are those of the 22-kW induction machine in [4]. In order to investigate the frequency responses of the double-cage rotor circuits, the rotor resistance and leakage inductance of the single equivalent circuit in Fig. 2 are derived as (17) and (18). Analytically derived expressions are given for the values of each of the double-cage circuit elements. Using (17) and (18), the frequency responses of the double-cage rotor can

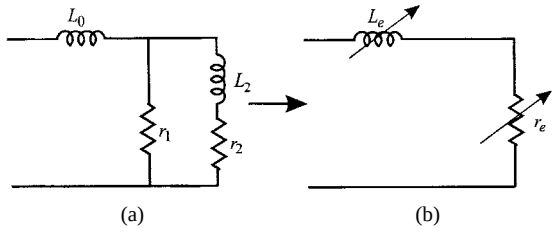

Fig. 2. Relationship between double-cage and single-cage rotor.

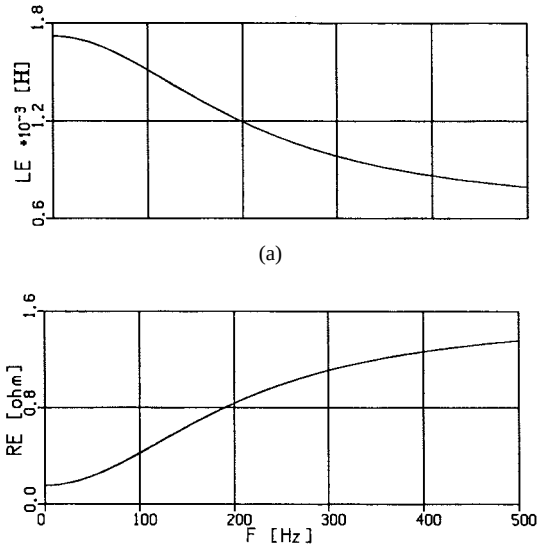

Fig. 3. Variation of rotor parameters versus frequency.

TABLE I
SELECTED ROTOR PARAMETERS OF DOUBLE-CAGE INDUCTION MACHINE UNDER SIMULATION

Upper cage resistance r_1	1.562 Ω
Lower cage resistance r_2	0.172 Ω
L_0	0.636 mH
L_2	1.337 mH

be illustrated as in Fig. 3(a) and (b). These graphs reflect the true nature of skin effect in the double-cage model:

$$r_e(\omega) = \frac{r_1 r_2 (r_1 + r_2) + r_1 \omega^2 L_2^2}{(r_1 + r_2)^2 + \omega^2 L_2^2} \tag{17}$$

$$L_e(\omega) = \frac{(r_1 + r_2)(r_1 L_2 + r_1 L_0 + r_2 L_0) - L_2 (r_1 r_2 - \omega^2 L_0 L_2)}{(r_1 + r_2)^2 + \omega^2 L_2^2}. \tag{18}$$

The use of a single effective rotor resistance and leakage inductance implies that it can be only defined for one rotor frequency, normally the fundamental slip frequency. In transient state, for example, this is the case where, during the starting of the machine and under load changes, the effective rotor resistance is much greater than its dc value and rotor leakage inductance is reduced. However, the transient state

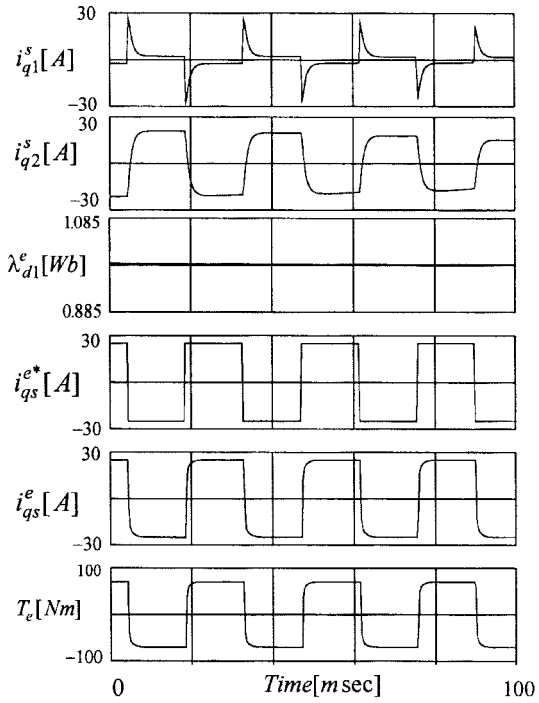

Fig. 4. Machine torque dynamics for rectangular shape command.

inducing high-frequency component into the rotor cage current only lasts a few milliseconds, as shown in Fig. 4, even in the case of rapid reversal of the torque. Since the current could follow the reference current by a current regulator as quickly as possible, in a vector-controlled induction machine, the rotor frequency is limited to a fundamental slip frequency except for a few milliseconds, as shown in Fig. 4, and the effective rotor resistance r_{re} is almost equal to the parallel combination of the upper and lower resistance, as in

$$r_{re} = \frac{r_1 r_2}{(r_1 + r_2)}. \tag{19}$$

To investigate the deep-bar effect according to a transient component current in the rotor, the torque command with a rectangular shape is applied to the machine with the deep-bar rotor, the parameters of which are listed in Table I. The value of equivalent rotor resistance r_{re} in the controller is given as 0.1549 Ω from (19).

Fig. 4 clearly shows that most of rotor current is the lower cage current i^s_{q2} in steady state and the upper cage current i^s_{q1} for a few milliseconds. The torque command is a half-rated value, and its frequency is 35 Hz. In Fig. 4, pseudorotor flux λ^e_{d1} is controlled to maintain constant flux level, and the machine torque T_e can respond perfectly to step q-axis current command $i^{e^*}_{qs}$. When a fast torque command is applied to the machine at standstill, the rotor currents of upper and lower cage in the stationary frame, i^s_{q1} and i^s_{q2}, have a high-frequency component during the transient state. Even though a high-frequency current is injected into the rotor branch, the equivalent rotor resistance at transient state is not much detuned compared to that at steady state obtained from the pseudorotor-flux-oriented control concept.

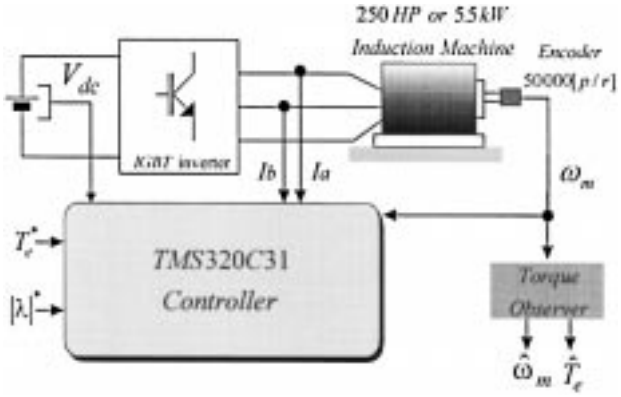

Fig. 5. Experimental system configuration.

TABLE II
RATINGS AND PARAMETERS OF INDUCTION MACHINE UNDER TEST

Rated power output	250 HP	5.5 kW
Rated torque(Nm)	1016	30
Rated line voltage(V)	440	170
Number of pole	4	4
Rated supply frequency(Hz)	60	60
Moment of inertia($Kg-m^2$)	4	0.038
Stator resistance(Ω)	0.013	0.232
Rotor resistance(Ω)	0.075	0.12
Mutual inductance(mH)	12	36.3
Stator transient inductance(mH)	0.2	2.3

V. EXPERIMENTAL RESULTS

Extensive tests are performed to evaluate the feasibility of the presented study. The algorithm is programmed and installed on actual IGBT inverters to drive a 250-hp induction machine and 5.5-kW double-cage machine. The parameters of these machines were already known for the indirect rotor-flux-oriented control , and their accuracy was verified by laboratory tests. Table II shows such known parameter values.

The switching devices in the inverter are IGBT's with 4-kHz switching frequency. The dc-link voltage is 600 V for the 250-hp machine and 300 V for double-cage machine, receptively, and the sampling period of current control is 125 μs. The cutoff frequency of the flux controller is 10 rad/s for the 250-hp machine and 5 rad/s for the double-cage machine. The cutoff frequency of the torque controller is selected to be 2000 rad/s for both machines. In order to ensure the validity of the proposed algorithm, it is required to measure the actual machine torque. An ideal method would be to calculate the torque by differentiating the mechanical speed, but direct differentiation enlarges the noise component. Therefore, the torque observer is used to monitor the actual torque [8].

Due to the fact that fast and accurate measurement of mechanical speed is very critical for the estimation of instantaneous torque, a high-resolution encoder is attached to the motor shaft in Fig. 5. A TMS320C31 digital signal processor (DSP) is used as a main control processor, which operates at 33.33-MHz clock speed and is capable of 33.33 million floating-point operations per second.

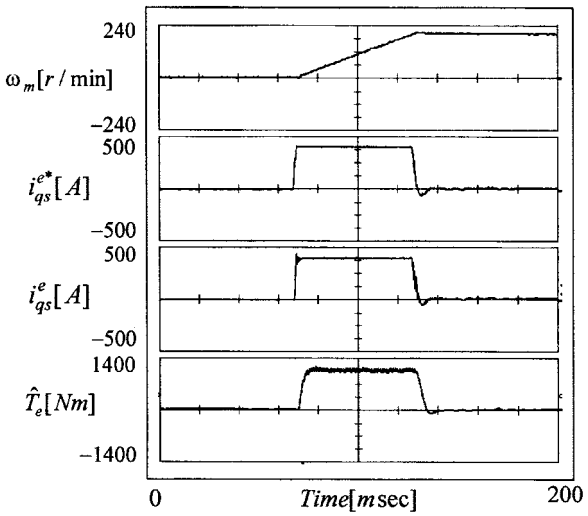

Fig. 6. Static characteristic of machine torque.

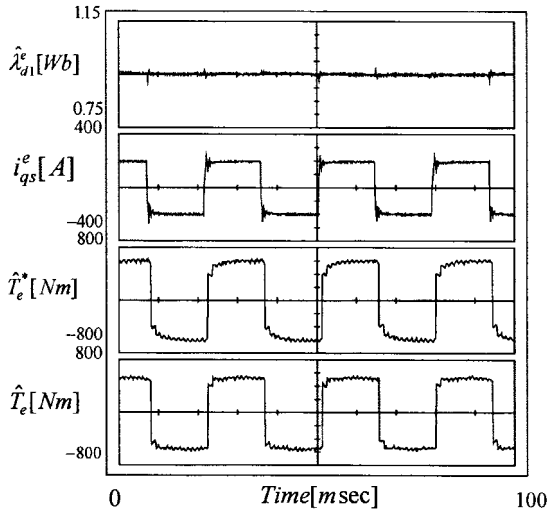

Fig. 7. Machine torque dynamics for rectangular shape command.

A. 250-HP Induction Machine for Vector Control Operation

The sampling time of the speed detection is about 1 ms, and the observer is designed to have a 200-Hz cutoff frequency. The measurement speed error for the worst case is less than 0.006 r/min at 200 r/min, and this error corresponds to 5 N·m or 0.005 p.u. of rated torque.

Fig. 6 shows the actual waveforms of mechanical speed, q-axis current command, q-axis current, and estimated torque from top to bottom. The speed command changes from 0 to 200 r/min, and the static torque perfectly responds to torque command. The rotor parameters in the controller are equivalent rotor parameters derived from the pseudorotor-flux-oriented control scheme. In this case, the frequency of rotor currents is limited to a few hertz, corresponding to the controlled slip frequency.

To examine the torque dynamics according to a high-frequency injection, another test is performed on the 250-hp

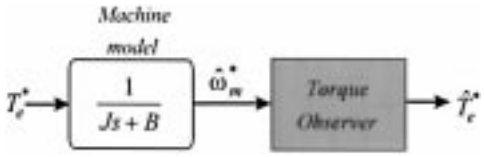

Fig. 8. Schematic representation of $\hat{T}_e^*$ calculation.

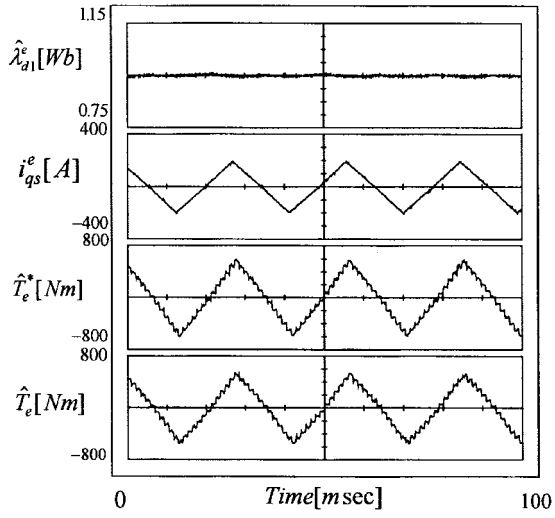

Fig. 9. Machine torque dynamics for triangular-shape command.

machine. The amplitude of the signal is selected as 60% of rated torque. Considering the torque observer dynamics, the working frequency of the injection signal is selected as 35 Hz. The result is illustrated in Fig. 7 and pseudorotor flux $\hat{\lambda}_{d1}^e$ is controlled to maintain constant flux level. In order to evaluate the effect of the observer for the torque estimation, torque command T_e^* is processed through the same observer, and its result is shown as $\hat{T}_e^*$ in Fig. 8. The two traces of $\hat{T}_e^*$ and $\hat{T}_e$ are almost identical, as shown in Fig. 7. By this fact, it can be concluded that the generated torque T_e is almost identical to the commanded torque T_e^* and that the deep-bar effect is negligible in a practical sense.

To verify the above conclusion once more, a triangular-wave test with the same frequency and amplitude as those of Fig. 7 is performed. Fig. 9 shows the test signal and its result. The estimated machine torque is well controlled, without any dynamic deterioration. Generally, in large machines, the rotor leakage reactance value becomes low compared to that of rotor resistance. Therefore, even though a high-frequency current is injected into the rotor branch, the distribution of rotor current in the transient state is not much changed compared to that of rotor current in the steady state. This corresponds to a rotor parameters error less than 20% in the case of the machine test frequency. Moreover, this kind of signal, which has high current level and frequency, is seldom used in practical application.

B. 5.5-kW Double-Cage Induction Machine

In order to ensure the validity of the proposed control scheme, other tests are performed on a double-cage machine, the impedance locus of which fits closely to that of the deep-bar machine. The detailed rotor shape provided by the manufacturer is shown in Fig. 10, and its dimensions are given in Table III. The sampling time of the speed measurement is about 1 ms and the observer is designed to have a 200-Hz cutoff frequency. The measurement speed error for the worst case is less than 0.03 r/min at 500 r/min, and this error corresponds to 1.2 N·m or 0.04 p.u. of rated torque.

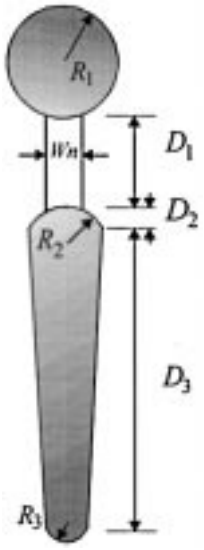

Fig. 10. Rotor shape of double cage machine under test.

TABLE III
ACTUAL DIMENSIONS OF DOUBLE-CAGE INDUCTION MACHINE UNDER TEST

Dimension	Value(mm)
R_1	2.25
R_2	1.75
R_3	0.9
W_n	1.5
D_1	3.998
D_2	1.75
D_3	10.831

Fig. 11 shows the actual waveforms of mechanical speed, q-axis current command, q-axis current, and estimated torque from top to bottom. The speed command changes from 0 to 500 r/min, and the static torque perfectly responds to the step torque command. The rotor parameters in the controller are equivalent rotor parameters derived from the pseudorotor-oriented control scheme. In the double-cage machine, the upper cage is usually designed to yield a relatively high starting torque and limit a starting current. However, in the vector-controlled operation, the slip frequency is controlled in a few hertz and, so, the rotor parameters considering the concept of the pseudorotor-flux-oriented control can be used in the controller.

To examine the torque dynamics according to a high-frequency injection, another test is performed similar to the 250-hp machine. The amplitude of the signal is selected as 40% of rated torque and frequency as 35 Hz. The result is

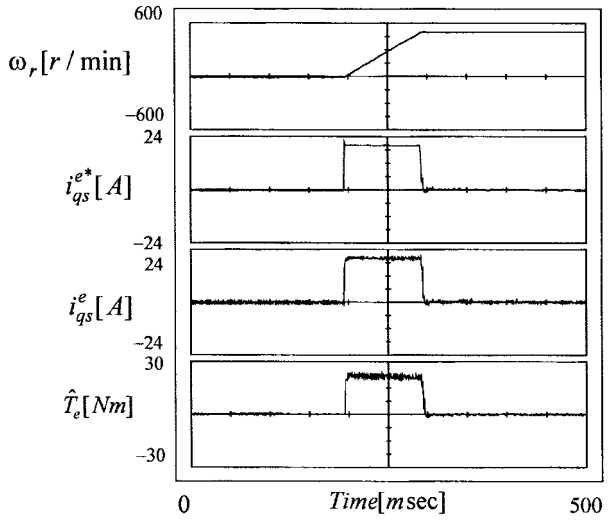

Fig. 11. Static characteristic of double-cage machine torque.

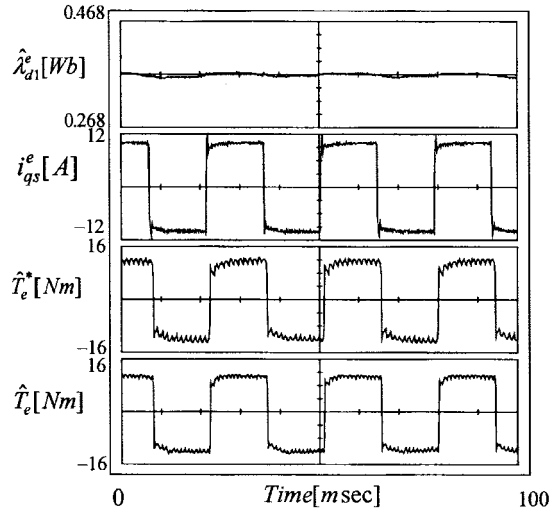

Fig. 12. Double-cage machine torque dynamics for rectangular shape command.

illustrated in Fig. 12, and pseudorotor flux $\hat{\lambda}_{d1}^{e}$ is controlled to maintain constant flux level. In order to monitor the observer characteristic for the torque command, $\hat{T}_e^*$ is estimated as shown in Fig. 8. The responses of $\hat{T}_e^*$ and $\hat{T}_e$ are almost the same, and this clearly shows that the deep-bar effect is negligible, even in the vector-controlled double-cage machine when parameters are reasonably accurate.

VI. Conclusions

Introducing an indirect pseudorotor-flux-oriented control scheme, the conventional rotor-flux-oriented control using equivalent rotor parameters are effective for deep-bar and/or double-cage machine. The approach has been validated using a 250-hp induction machine for vector control operation and a high-precision torque observer. In order to show clearly the validity of the proposed study, some tests were performed on a 5.5-kW double-cage induction machine, impedance locus of whch closely fits that of the deep-bar machine. The deep-bar effect on the field-oriented control of the induction machine can be neglected in a practical sense if the proper flux is selected for orientation.

References

[1] E. Levi, *Polyphase Motors*. New York: Wiley, 1984.
[2] W. Levi, C. F. Landy, and M. D. McCulloch, "Improved models for the simulation of deep bar induction motors," *IEEE Trans. Energy Conversion*, vol. 5, pp. 393–400, June 1990.
[3] P. L. Alger, *The Nature of Induction Machines*. New York: Gordon and Breach, 1965.
[4] R. W. A. A. De Doncker, "Field-oriented controller with rotor deep bar compensation circuits," *IEEE Trans. Ind. Applicat.*, vol. 28, pp. 1062–1071, Sept./Oct. 1992.
[5] R. C. Healey, S. Williamson, and A. C. Smith, "Improved cage rotor models for vector controlled induction motors," *IEEE Trans. Ind. Applicat.*, vol. 31, pp. 812–822, July/Aug. 1995.
[6] A. C. Smith, S. Williamson, and R. C. Healey, "A transient induction motor including saturation and deep bar effect," *IEEE Trans. Energy Conversion*, vol. 11, pp. 8–15, Mar. 1996.
[7] P. Vas, *Vector Control of AC Machines*. London, U.K.: Oxford Univ. Press, 1990, pp. 122–215.
[8] S. J. Kang and S. K. Sul, "Direct torque control of brushless DC motor with nonideal trapezoidal back EMF," *IEEE Trans. Power Electron.*, vol. 10, pp. 796–802, Nov. 1995.

Jul-Ki Seok (S'94) received the B.S., M.S., and Ph.D. degrees in electrical engineering from Seoul National University, Seoul, Korea, in 1992, 1994, and 1998, respectively.

Since 1998, he has been with the Production Engineering Center, Samsung Electronics Company, Ltd., Suwon City, Kyungki-Do, Korea. His research interests include electrical machines, high-performance electric machine control, and high-power ac drives.

Seung-Ki Sul (S'78–M'80–SM'98) received the B.S., M.S., and Ph.D. degrees in electrical engineering from Seoul National University, Seoul, Korea, in 1980, 1983, and 1986, respectively.

He was with the Department of Electrical and Computer Engineering, University of Wisconsin, Madison, as a Research Associate from 1986 to 1988. From 1980 to 1990, he was a Principal Research Engineer with Gold-Star Industrial Systems Company. Since 1991, he has been with the Department of Electrical Engineering, Seoul National University. His present research interests are in high-performance electric machine control using power electronics. He is currently performing various research projects for industrial systems, and some of the results are applied to the field of industrial high-power electric machine control.